Applied Catalysis B: Environmental 165 (2015) 222–231

Contents lists available at ScienceDirect

Applied Catalysis B: Environmental

journal homepage: www.elsevier.com/locate/apcatb

Mechanochemical synthesis of copper manganese oxide for the ambient temperature oxidation of carbon monoxide

Tomos J. Clarke[a], Thomas E. Davies[b], Simon A. Kondrat[a], Stuart H. Taylor[a,*]

[a] Cardiff Catalysis Institute, School of Chemistry, Cardiff University, Main Building, Park Place, Cardiff CF10 3AT, UK
[b] Stephenson Institute for Renewable Energy, Chemistry Department, University of Liverpool, Crown Street, Liverpool L69 7ZD, UK

ARTICLE INFO

Article history:
Received 13 June 2014
Received in revised form
15 September 2014
Accepted 26 September 2014
Available online 6 October 2014

Keywords:
Copper manganese oxide
Carbon monoxide
Oxidation
Mechanochemical grinding

ABSTRACT

A series of copper manganese oxide catalysts have been prepared by mechanochemical grinding of carbonate precursors and tested for the low temperature oxidation of CO. It is shown that a 72 h grind time and heat treatment under oxygen is necessary to form active $CuMn_2O_4$ for the conversion of CO to CO_2 at room temperature. Energy dispersive X-ray analysis mapping indicated that the degree of mixing was improved at longer grinding times. Contraction of the $MnCO_3$ lattice, followed by X-ray diffraction, showed that grinding times in excess of 24 h were necessary for the near complete dissolution of Cu ions into the $MnCO_3$ framework, which in turn facilitated the formation of $CuMn_2O_4$ upon calcination. This simple, clean and environmentally friendly synthesis shows how mixed metal oxides that are catalytically active at room temperature can be synthesized without employing aqueous precipitation techniques, which result in waste streams containing carbonate and nitrate contaminants.

1. Introduction

The tenets of green chemistry include the need for one-step environmentally friendly synthesis routes using benign precursors, which generate little or no waste streams. Reactive grinding or mechanochemical synthesis of catalysts is a growing area in the field of materials chemistry and offers a simple and waste free preparative route [1]. It offers a number of advantages when compared to some traditional methods. The process is environmentally friendly and economically efficient as there are no solvents used, no waste from washing, fewer synthesis steps, and no requirement for product recovery or separation. Catalyst poisons such as Na^+, K^+ and Cl^- from precipitating agents are also minimised [2]. In addition, the catalytic activity can be enhanced by virtue of the increased contact through grain boundaries [3], introduction of stacking faults [4], as well as the increase in surface area as a result of a decrease in particle size [5].

Single metal oxides are the simplest catalysts to prepare by a mechanochemical route; examples include catalysts which are highly active for the oxidation of volatile organic compounds and the degradation of pollutants. Catalysts such as Co_3O_4 have been synthesised and tested for total oxidation of propane with excellent low temperature activity, which is linked to the small particle size afforded by the grinding and rapid crystallisation [6,7]. In other examples, ZnO and TiO_2 catalysts have been prepared and tested for photocatalytic reactions. ZnO was tested for the decomposition of benzene-1,3-diol and showed activity comparable to other catalysts in the literature[8]. Whereas TiO_2 and carbon doped TiO_2 showed improved activity for the photocatalytic generation of hydroxyl radicals and the decomposition of NO_x respectively [9,10].

Mechanochemical synthesis of mixed metal oxides can be more problematic, due to the difficulty in achieving a well mixed homogeneous distribution of the active components, although it can be achieved. Copper based catalysts for the steam reforming of methanol, such as $Cu_3Fe_4(VO_4)_6$ [11], Cu/Al_2O_3 [12] and Cu/ZnO [13–15] have received a lot of attention, possibly due to the industrial relevance of the catalyst. In many cases it was found that the activity of the catalysts was linked to the length of the grinding time, as it increased dispersion, decreased particle size and consequently increased surface area. Molybdenum zeolites have been prepared by mechanochemical methods and they are active for hydrodesulfurization [16], but they were not as active as when prepared by impregnation. Mechanochemically prepared ceria and titania supported gold catalysts have also been shown to be active for preferential oxidation of CO [17] and liquid phase oxidations [18], but again the dispersion and particle size of the active phase were difficult to control. Perovskites have been synthesised by reactive grinding and tested for alkane activation and total oxidation. It was

* Corresponding author. Tel.: +44 29 2087 4062.
E-mail address: taylorsh@cardiff.ac.uk (S.H. Taylor).

http://dx.doi.org/10.1016/j.apcatb.2014.09.070
0926-3373/

found that the unprecedented high surface areas of >100 $m^2 g^{-1}$ along with the increased defect density led to increased activity when compared to a perovskite prepared by a more traditional citrate complex method [19,20].

Mixed metal oxides of the spinel and inverse spinel type have long been synthesised by a variety of methods and investigated primarily for their catalytic, electronic, optical and magnetic properties [21,22]. An example of such a material is copper manganese oxide (Hopcalite), first investigated in the early 20th century. It is a well studied and commercially available catalyst proven to be active for a large number of oxidation reactions [23]. Commercial varieties of Hopcalite have been synthesised by a solid-state reaction between active components MnO_2 and CuO, with additional binders and promoters such as AgO_2 [24]. More active catalysts can be prepared by other routes such as co-precipitation [25–27], sol-gel [28] and precipitation by supercritical CO_2 [29], but can be limited in their application due to the more complex preparation methods when compared to the simple solid state reaction between the metal oxides.

In this study we have investigated the preparation of Hopcalite and show how additive free mechanochemical grinding of the precursor carbonates can facilitate the preparation of Hopcalite. In particular, we were interested in the potential incorporation of Cu^{2+} ions into the $MnCO_3$ framework in an attempt to increase the rate of copper manganese oxide formation during heat treatment. Carbonates have been used as precursors, as previously we have shown that more active materials with higher surface areas are formed by virtue of the endothermic decomposition of the carbonate precursor during calcination [30,31]. Conversely, the use of precursors that decompose exothermically can lead to phase separation and preferential reduction of one or more of the active components [32]. This effect has an important influence on the catalyst activity for low temperature carbon monoxide oxidation. In this work we have studied the relationship between the mechanochemical preparation variables, catalyst structure and activity.

2. Experimental

2.1. Catalyst preparation

Catalysts were prepared using a planetary ball milling method. A Retsch PM100 planetary ball mill with a 10 cm zirconia grinding vessel with six 15 mm zirconia grinding balls was used. All grinding was performed at 25 °C. Powdered $Cu_2(OH)_2CO_3$ (Sigma Aldrich, 95%) and $MnCO_3$ (Sigma Aldrich, 99.9%) were mixed in a 1:2 copper to manganese molar ratio. The powders were ground for varying periods of time (0.5–72 h) at 400 rpm. The resulting dry solid powders were recovered and calcined in static air (415 °C for 2 h with a ramp rate of 2 °C min^{-1} from ambient temperature [26]). After calcination samples were stored in a desiccator to prevent water adsorption. Copper oxide and manganese oxides were prepared by grinding the reagents individually for 1 h by the same method. The commercial catalyst tested was stored in a desiccator to prevent water adsorption.

2.2. Catalyst characterisation

The catalysts were characterized by powder X-ray diffraction (XRD) using a Panalytical X'Pert diffractometer, using a Cu source operating at 40 kV and 40 mA. The phases present were confirmed by matching patterns to the ICDD database. Crystallite sizes were determined by using the Scherrer equation. Lattice parameters were determined by Reitveld analysis using Panalytical Highscore plus software. The peak profiles were fitted using pseudo-Voigt function and the parameters were refined in the order of scale factors, zero shift, cell parameters, thermal parameters peak shape function and preferred orientation. *In situ* XRD analysis of the uncalcined catalysts was undertaken using a Panalytical X'Pert Pro diffractometer fitted with an Anton Paar 900 K *in situ* cell. An X-ray diffractogram of the precursor was taken at room temperature before heating the sample to 600 °C at a heating rate of 2 °C min^{-1}. Air was flowed through the sample cell at a rate of 4 mL min^{-1}. The heating profile was paused every 25 °C between 175 and 600 °C to acquire diffractograms of the sample as it decomposed to form the calcined catalyst.

The surface area of the catalysts was determined using a Micromeritics Gemini 2360 analyser. The catalysts were pretreated under a flow of N_2 at 120 °C for 30 min prior to analysis. The surface area was determined by 5-point N_2 adsorption at −196 °C and the data analysed using the BET method.

Temperature programmed reduction (TPR) analysis of the catalysts was performed using a Quantachrome ChemBET TPD/R/O apparatus. Hydrogen consumption was measured as 30 mg of the catalyst was exposed to a flow of 10%H_2/Ar at a flow rate of 30 mL min^{-1} whilst heating from ambient to 600 °C at a rate of 15 °C min^{-1}. Thermal gravimetric analysis (TGA) was performed using a Seteram Labsys TGA/DTA apparatus. Mass loss and heat flow for the catalyst precursors were examined over a temperature range of 30–600 °C under an atmosphere of flowing air (30 mL min^{-1}).

The morphology and elemental composition of powdered catalysts were evaluated by scanning electron microscopy (SEM) using a Jeol-6610LV equipped with an Oxford Instruments energy dispersive X-ray (EDX) analyser. Samples were gold coated using a Quorum Q150T ES sputter coater. Transmission electron microscopy (TEM) of the samples was undertaken using a JEOL 2100 microscope operating at 200 kV with a LaB_6 filament. Samples were mounted on 300 mesh copper grids covered in a holey carbon film. EDX measurements were performed using an Oxford Instruments $Xmax^N$ 80T detector.

In order to obtain elemental composition data on the materials Microwave Plasma Atomic Emission Spectroscopy (MP-AES) was performed using an Agilent 4100 MP-AES. The Cu and Mn content of each catalyst was measured using two emission lines for each metal, 324 nm and 327 nm for Cu with 403 and 404 nm used for Mn. The samples were introduced to the nitrogen plasma using a single pass spray chamber at a pressure of 240 kPa without air injection. A known amount of each catalyst precursor was dissolved in 5 mL aqua regia then diluted up to 50 mL using deionized water. A 10% aqua regia rinse solution was introduced between samples for 15 s to ensure there was no sample contamination. Each sample was run 3 times with the average result used to determine the Cu:Mn ratio.

The instrument was calibrated with standards of appropriate concentration containing both Cu and Mn in a 10% aqua regia solution along with a 10% aqua regia blank.

2.3. Catalyst testing

The catalysts were tested for CO oxidation using a fixed-bed microreactor. The reaction temperature was maintained isothermally at 25 °C by immersing the U-shaped reactor tube in a thermostatically controlled water bath. 5000 vppm CO in air and a gas hourly space velocity of 12,000 h^{-1} (50 mg catalyst, flow rate 21 ml min^{-1}) was used. Analysis of reactants and products was performed using on-line gas chromatography (Varian CP-3800) with a Supelco Carbosieve column (3 m × 35 mm) with a thermal conductivity detector. Conversion was calculated on the basis of CO_2 formation and the detector was calibrated using standard gas mixtures.

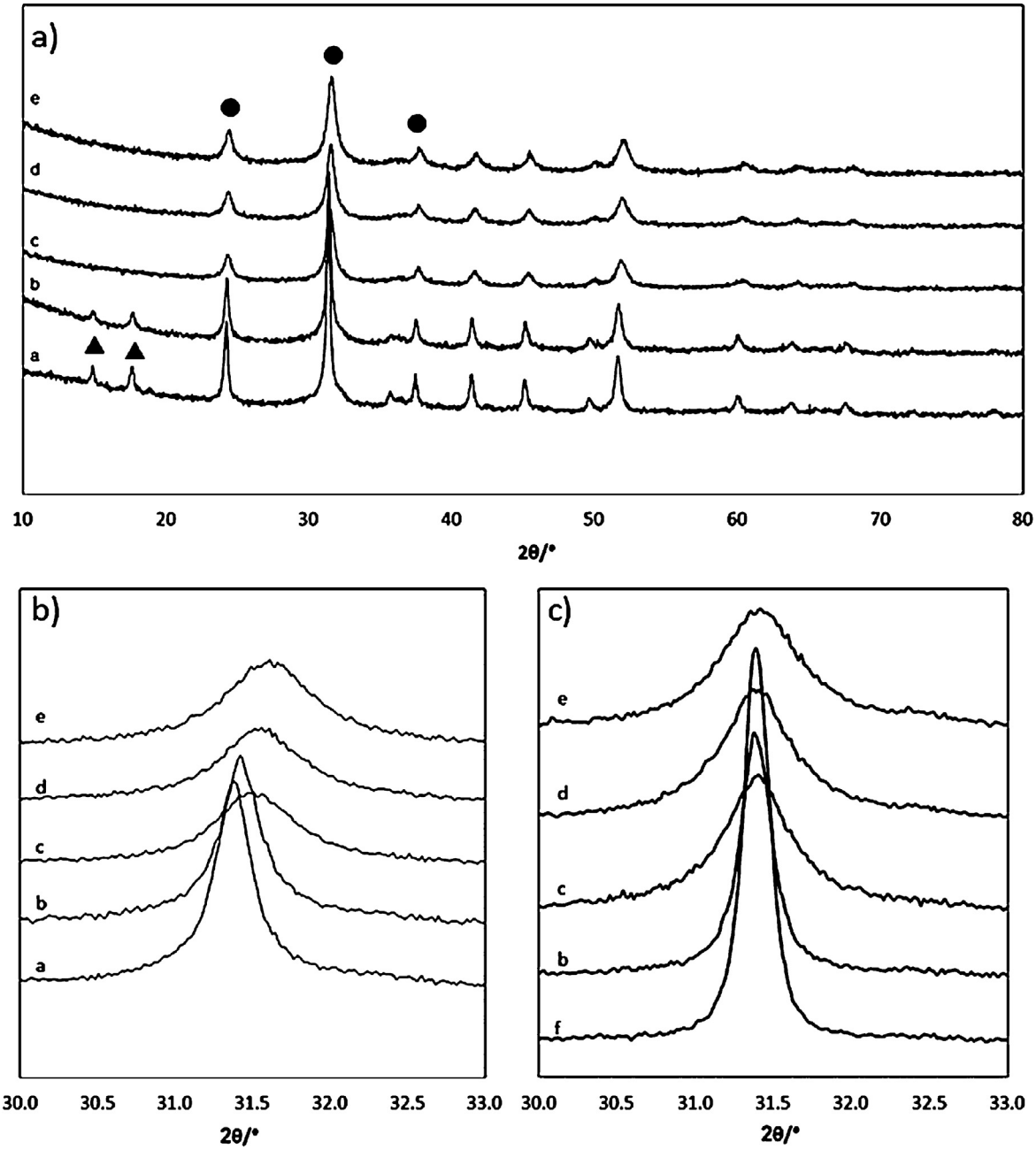

Fig. 1. (a) Powder XRD patterns of the $MnCO_3$ and $Cu_2(OH)_2CO_3$ physical mixture milled for different times. (b) Shift in $MnCO_3$ [1 0 4] reflection to higher 2θ values. (c) $MnCO_3$ ground in absence of $Cu(OH)_2CO_3$ showing no shift in the [1 0 4] peak. In all figures; (a) 0.5 h, (b) 1 h, (c) 12 h, (d) 24 h, (e) 72 h, (f) Unground: ● $MnCO_3$, ▲ $Cu(OH)_2CO_3$.

3. Results and discussion

The XRD patterns of the catalyst precursors prepared by grinding the carbonates together are shown in Fig. 1. Diffraction from the hexagonal-rhombohedral structure of $MnCO_3$ is dominant, indicated by the main (1 0 4) reflection at 31.4° 2θ. Initially the (0 2 0) and (1 2 0) reflections from the $Cu_2(OH)_2CO_3$ are also clearly visible at 14.9 and 17.6° 2θ, respectively. After 1 h of grinding there was a decrease in the $Cu_2(OH)_2CO_3$ (0 2 0) and (1 2 0) peak intensities, which after 12 h grinding were no longer visible. This indicates a reduction of crystallite size, loss of crystallinity or a phase change, possibly to form a $Cu_xMn_{1-x}CO_3$ type solid solution. XRD analysis of individually ground $Cu_2(OH)_2CO_3$ (Figure S1) also showed that the reflections disappeared with grinding time, again suggesting reduction of crystallite size or possibly loss of crystallinity. Correspondingly, in the mixed carbonate system, with the loss of reflections from the Cu phase, there was a shift in the positions of the $MnCO_3$ (1 0 4) reflections to higher 2θ values, indicating a contraction of the lattice parameter of the $MnCO_3$ unit cell (Fig. 1b). Table 1 shows the changes of lattice parameters of $MnCO_3$ as a function of grinding time. For the pure $MnCO_3$ phase the lattice constants a and c are 4.799 and 15.678 Å respectively, decreasing to 4.766 and 15.576 Å after 72 h milling. Grinding the pure $MnCO_3$ for the same amount of time showed no change in the peak position or lattice parameters as a function of grinding time (Fig. 1c), indicating that the decrease in unit cell volume is most likely a result of copper incorporation. Over the course of the grinding period the cell volume decreased from 312.82 $Å^3$ to 306.25 $Å^3$. This effect has been

Table 1
Physical properties and lattice parameters of manganese carbonate and copper carbonate after grinding for varying times.

Grinding Time (h)	Crystallite size (nm)	Cell parameters				TGA				Calcined surface area ($m^2 g^{-1}$)	MP-AES Cu:Mn ratio
		a (Å)	*b* (Å)	*c* (Å)	Vol (Å)	Mass loss (%)		Temperature of mass loss (°C)			
						1	2	1	2		
$MnCO_3$	61	4.7993	–	15.6783	312.824	–	–	–	–	–	
CuO	–	–	–	–	–	–	–	–	–	13	
MnOx	–	–	–	–	–	–	–	–	–	60	
0.5	35	4.7983	–	15.6666	312.380	8	16	300	495	65	1:1.84
1	27	4.7985	–	15.6693	312.367	6	16	307	483	45	1:1.83
12	15	4.7717	–	15.6086	307.629	–	21	–	480	50	1:1.83
24	14	4.7690	–	15.5901	306.954	–	22	–	475	21	1:1.86
72	14	4.7664	–	15.5757	306.451	–	21	–	438	78	1:1.84

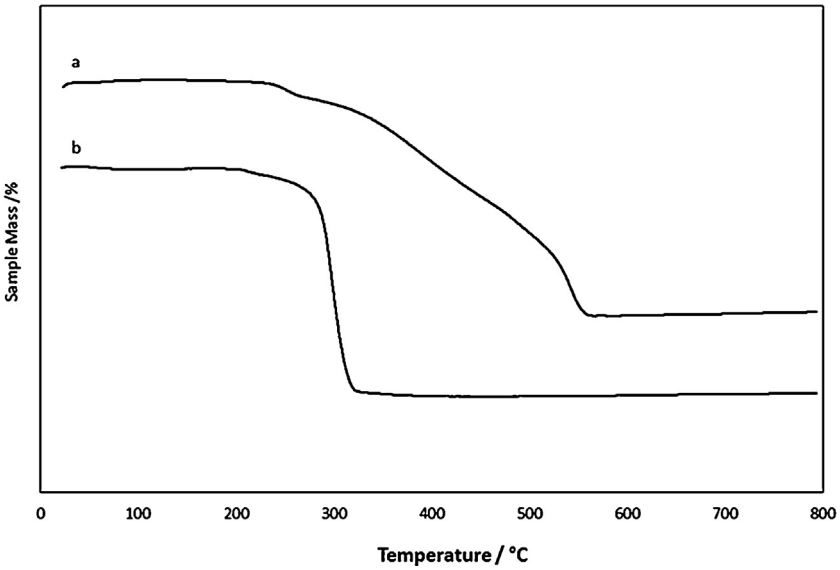

Fig. 2. Thermogravimetric analysis of unground precursors (a) $MnCO_3$ and (b) $Cu_2(OH)_2CO_3$.

observed previously and is associated with the incorporation of Cu^{2+} ions into the $MnCO_3$ lattice, which has been determined to be more facile than incorporation of Mn into $Cu_2(OH)_2CO_3$. Previous studies by Porta et al. indicated that the incorporation of Cu^{2+} into the $MnCO_3$ lattice was limited to *ca.* 30%. In this case the decrease in unit cell volume of *ca.* 6 $Å^3$ implies that not all the Cu present is fully incorporated into the lattice, and the incorporation is *ca.* 15%. The large decrease in cell volume is not solely related to the smaller

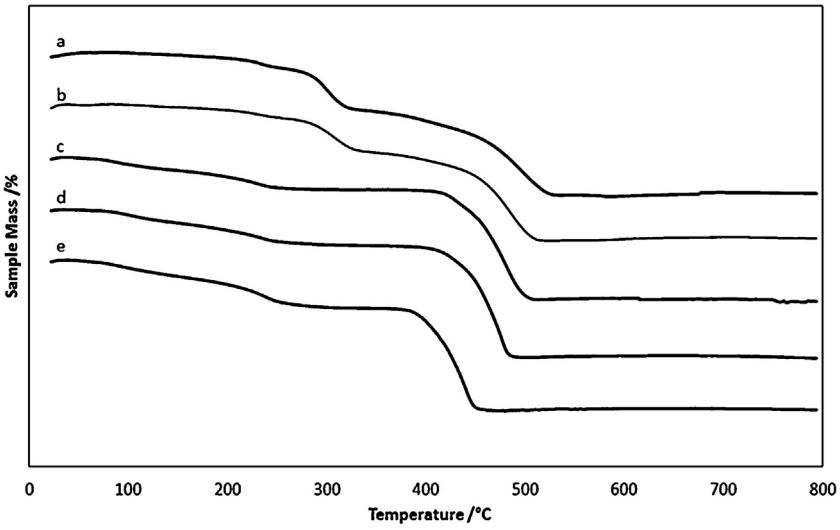

Fig. 3. Thermogravimetric analysis of precursors prepared by grinding for various times: (a) 0.5 h, (b) 1 h, (c) 12 h, (d) 24 h, (e) 72 h.

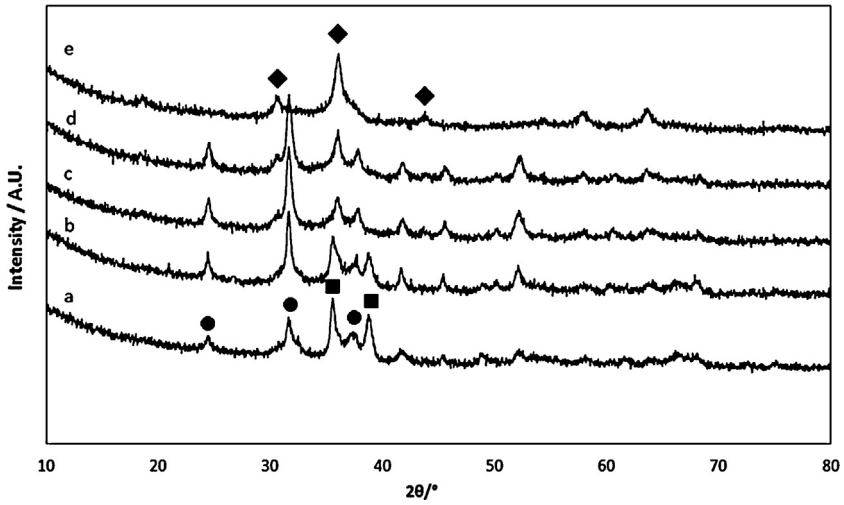

Fig. 4. Powder XRD patterns of catalysts prepared from precursors with various grinding times by calcination at 415 °C for 2 h; (a) 0.5 h, (b) 1 h, (c) 12 h, (d) 24 h, (e) 72 h: ● $MnCO_3$, ■ CuO, ♦ $CuMn_2O_4$.

Cu^{2+} ionic radius, but also to the higher local covalency of the CuO_6 polyhedra and site distortion, due to the d^9 electron configuration [33].

Table 1 shows the average crystallite size of the catalyst precursors. As would be expected the average $MnCO_3$ crystallite size decreased with increasing grinding time. The unground manganese carbonate has a crystallite size of 61 nm, this decreases with grinding to a minimum crystallite size of 14 nm after 24 h, further grinding had no further effect. This decrease in average crystallite size increases the rate of potential solid state reactions [34]. The

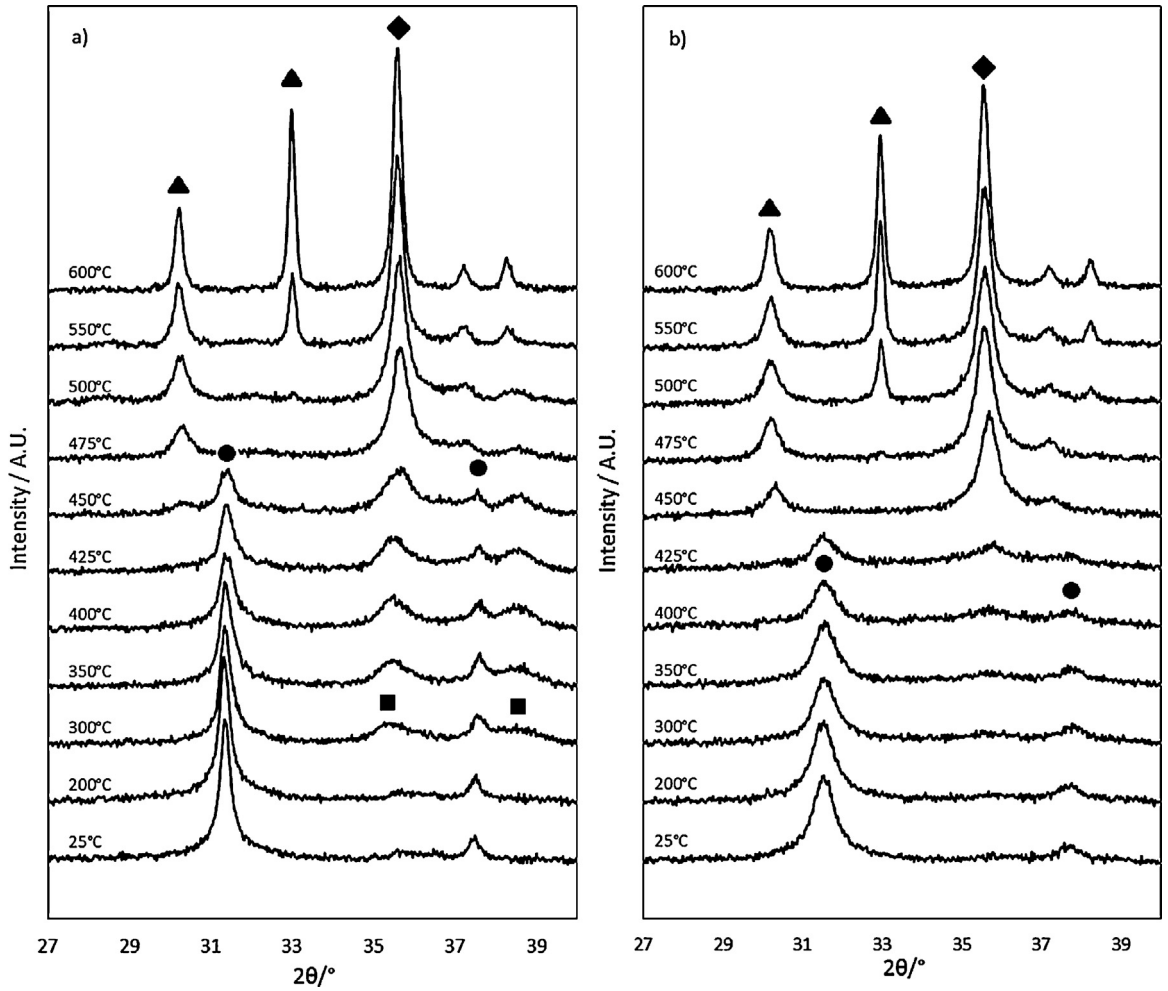

Fig. 5. *In situ* XRD of catalyst precursors heated under static air. (a) 1 h, (b) 72 h. Conditions: 25–600 °C, ramp rate of 2 °C min^{-1}, 17 min scan duration. ● $MnCO_3$, ■ CuO, ♦ $CuMn_2O_4$, ▲ Mn_2O_3.

smaller crystallite size should allow for more facile atomic diffusion of the Cu^{2+} into the lattice of the $MnCO_3$.

Thermal gravimetric analysis was also used to investigate the nature of the carbonate catalyst precursors. For comparison the TGA profiles of the starting copper and manganese carbonates are shown in Fig. 2, whilst profiles for the catalyst precursors prepared with varying grinding times are shown in Fig. 3. As was observed from the XRD, there was a distinct change in the properties of the materials when grinding time was increased from 1 to 12 h. At shorter grinding times (0.5–1 h) the mass loss profiles are similar, and can be interpreted as simply a combination of the individual carbonate profiles (Fig. 2) This consists of a well defined $Cu_2(CO_3)(OH)_2$ decomposition at *ca.* 300 °C overlaid with the gradual $MnCO_3$ decomposition between 300 and 550 °C.

After 12 h grinding the mass loss at 300 °C was less pronounced, with a continual weight loss from ambient up to 200 °C; this is attributed to loss of physisorbed water from the decomposition of $Cu_2(OH)_2(CO_3)$. Indeed, grinding of the individual $Cu_2(OH)_2CO_3$ under the same conditions resulted in a possible loss of crystallinity and the formation of amorphous materials with no reflections evident from XRD (Figure S1). The absence of the weight loss around 300 °C after 12 h grinding of the Cu Mn metal carbonate mixture is consistent with the XRD pattern (Fig. 1), which shows the disappearance of the $Cu_2(OH)_2CO_3$ phase. The increase of the relative weight loss between *ca.* 380 and 500 °C is also consistent with Cu^{2+} incorporation and formation of a $Cu_xMn_{1-x}CO_3$ type material. Also of note is the shift towards lower decomposition temperature of $Cu_xMn_{1-x}CO_3$ with increasing Cu^{2+} content, along with the mass loss becoming more rapid. Although it is evident from XRD that diffraction peaks from $Cu_2(OH)_2CO_3$ were no longer present in the longer grind times, the total weight loss for all samples was *ca.* 20%, which is very close to the theoretical value expected for transformation of the precursors to the oxides, indicating that very little, if any, H_2O or CO_2 was lost during the grinding process as a result of thermal effects.

The XRD patterns for the calcined catalysts (415 °C, for 2 h in air) are shown in Fig. 4. The phases present in the catalysts ground for 0.5 and 1 h were identified as $MnCO_3$ and CuO, There was no evidence of a crystalline $CuMn_2O_4$ phase. The retention of $MnCO_3$ corresponds with the broad temperature range seen for $MnCO_3$ phase decomposition, which extended up to *ca.* 500 °C (Fig. 3). Calcination of the precursor ground for 12 h resulted in the formation of $CuMn_2O_4$, with reflections associated with CuO no longer observed, but it was only after 72 h grinding that the reflections associated with $MnCO_3$ were no longer detected. The only observable phase in the calcined 72 h ground sample was nanocrystalline $CuMn_2O_4$. Furthermore, grinding of the individual $MnCO_3$did not result in any observable manganese oxide phases. $MnCO_3$ decomposition appears to coincide with $CuMn_2O_4$ formation, suggesting that Cu^{2+} incorporation into the $MnCO_3$ is responsible for the spinel phase formation. High Cu^{2+} incorporation and $MnCO_3$ thermal decomposition only occur after significant grinding time. This indicates that the process of atomic diffusion of Cu ions into the $MnCO_3$ framework is a relatively slow process and sufficient grinding time is required to achieve significant incorporation.

For comparison a commercial copper manganese oxide catalyst was also analyzed however the material showed no visible X-ray diffraction due to its amorphous/nanocrystalline nature.

Table 1 contains the surface area measurement for the calcined catalysts. The surface areas initially decreased with increased grinding time, from 65 $m^2\,g^{-1}$ after 0.5 h to 21 $m^2\,g^{-1}$ after 24 h. After 72 h the surface area increased to 78 $m^2\,g^{-1}$. The initial surface area decrease can be explained by the effect of sintering of the smaller crystallites of samples ground for longer periods into low surface area, copper oxide and manganese carbonate phases upon calcination. On the other hand, the sample ground for 72 h forms

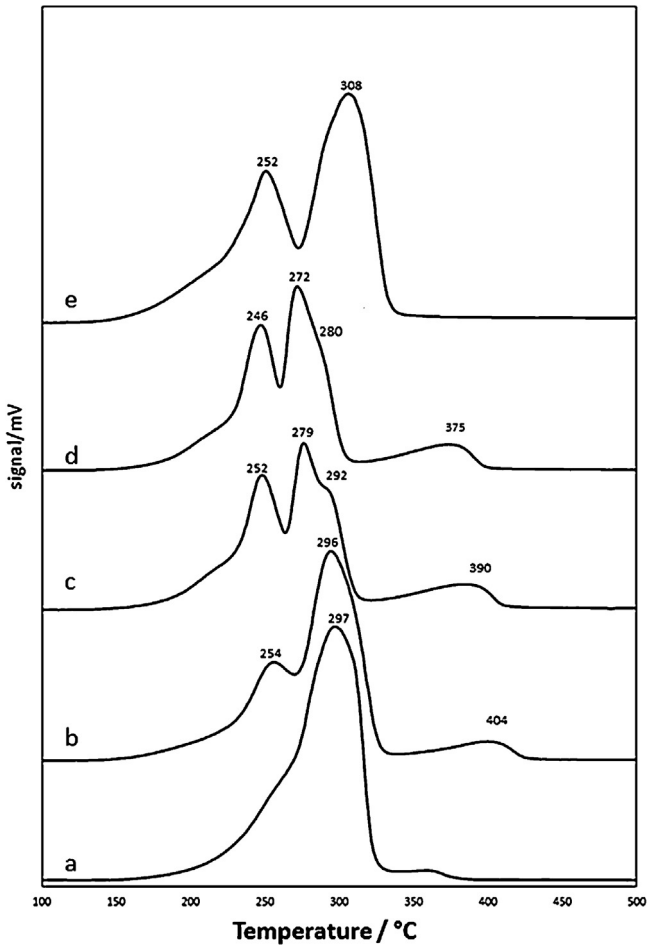

Fig. 6. Temperature programmed reduction profiles of catalysts calcined at 415 °C for 2 h prepared by varying grinding times: (a) 0.5 h, (b) 1 h, (c) 12 h, (d) 24 h, (e) 72 h.

the higher surface area $CuMn_2O_4$ spinel phase due to the increased incorporation of Cu^{2+} ions into the manganese lattice. The surface area of the commercial comparison catalyst was 140$m^2\,g^{-1}$, however, as the makeup of this catalyst is unknown it is not useful to draw a direct comparison.

As mentioned previously, XRD analysis of materials calcined at 415 °C did not show the presence of single metal oxides (CuO or Mn_2O_3) in conjunction with the mixed metal oxide spinel. *In situ* XRD was used in order to ascertain if single metal oxides, possibly produced at lower temperatures, react together to form the mixed metal oxide spinel, or if as suggested previously, crystalline $CuMn_2O_4$ formation coincides with $MnCO_3$ decomposition (Figs. 2 and 3). The two materials at the extremities of the grinding times, 1 h and 72 h, were investigated for comparison. A study of the phase formation over the temperature range from ambient to 550 °C for the catalyst precursors clearly illustrates the effect of increased grinding time. Fig. 5a shows the temperature dependent phase formation of the catalyst ground for 1 h. At 300 °C CuO reflections can be seen at 35.5° and 38.7° corresponding to the $(\bar{1}\,1\,1)$ and $(1\,1\,1)$ planes. This corresponds to the initial 300 °C mass loss, associated with $Cu_2(OH)_2CO_3$ decomposition, observed in the relevant TGA trace. Beginning at 450 °C, the $MnCO_3$ reflections (the principal reflection being 31.4°) decrease in intensity, whilst a reflection corresponding to $CuMn_2O_4$ is observed at 35.7°, associated with the $(3\,1\,1)$ lattice plane, and corresponds to the second mass loss observed in the TGA. At 500 °C reflections corresponding to Mn_2O_3 can be observed, principally the $(2\,2\,2)$ plane at 33.1°. This last phase

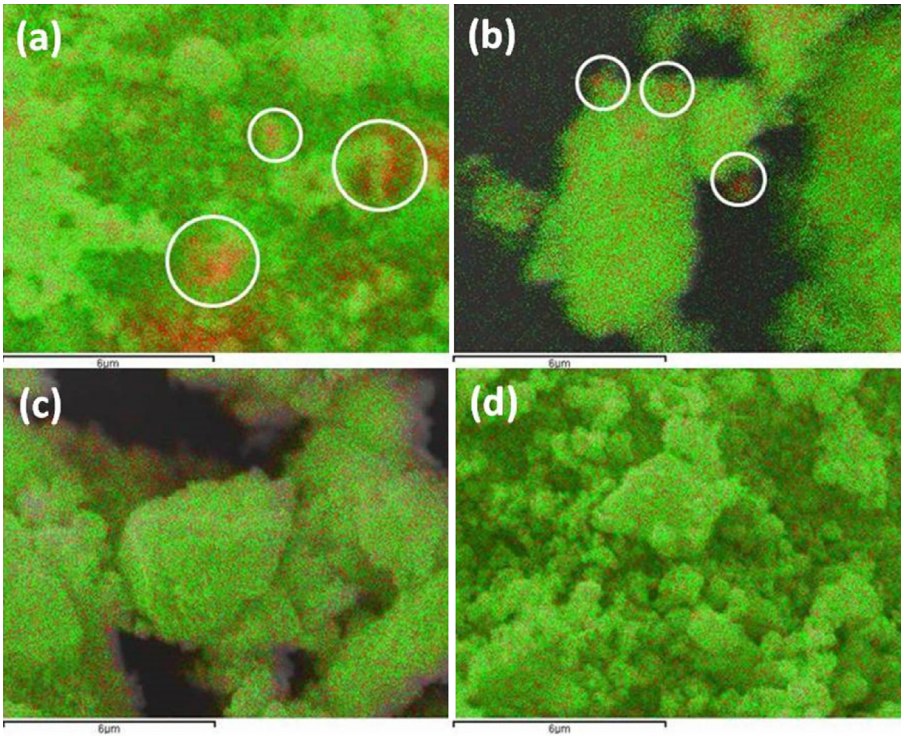

Fig. 7. Representative SEM-EDX mapping of catalysts calcined at 415 °C showing manganese (green) and copper (red). Circled areas show copper rich regions: (a) 0.5 h, (b) 1 h, (c) 24 h, (d) 72 h. (For interpretation of the color information in this figure legend, the reader is referred to the web version of the article.)

formation does not correspond with a mass loss in the TGA, suggesting that a highly disordered manganese oxide had already formed during the decomposition of $MnCO_3$.

Fig. 5b shows the *in situ* XRD analysis of the carbonates ground for 72 h. Unlike the previous example there is no evidence of CuO formation in the XRD. The characteristic peaks at 35.5° and 38.7° corresponding to the $(\bar{1}\,1\,1)$ and $(1\,1\,1)$ planes that are clear in Fig. 5a are not observed. It is our hypothesis that significant amounts of copper have been incorporated into the $MnCO_3$ lattice, limiting the amount available to form CuO. However, there would have to be a 33% Cu^{2+} incorporation into $MnCO_3$ to account for all of the Cu to be unavailable. As shown earlier, the $MnCO_3$ unit cell contraction suggested around 15% incorporation. Therefore, substantive amounts of a nanocrystalline or an amorphous Cu species must be present, at least until the point that mixed metal oxide spinel formation occurs. The XRD pattern of the $Cu_2(OH)_2CO_3$ ground in the absence of manganese carbonate (Figure S1) shows that after 72 h the material had no diffraction from significant crystalline domains. Calcination of this 72 h ground $Cu_2(OH)_2CO_3$ resulted in the formation of crystalline CuO by 300 °C (Figure S1). This shows that the Cu within the mixed metal oxide 72 h ground sample, which is not observable within the $MnCO_3$ lattice, must still be stabilised by the manganese phase. Interestingly, amorphous copper oxide hydrate minerals, such as Hydrocuprite and Melaconite, are known to be stabilized by manganese oxides [35]. This offers a precedent for the nature of the nanocrystalline amorphous copper phase present and stabilization in mixed manganese copper systems. The barrier for the migration of this amorphous copper material into forming manganese oxide phases would be lower than if the material was composed of large CuO crystallites. Therefore, it is difficult to unambiguously state that the presence of Cu^{2+} in the $MnCO_3$ lattice is the only source of spinel formation. However, what is clear is that prolonged grinding time improves the interfacial area between Cu and Mn, with the Cu being stabilised on or within the Mn phase. This is reflected in the ease of $CuMn_2O_4$ formation observed by *in situ* XRD, with a broad reflection at 35.7°, corresponding to $(3\,1\,1)$ lattice planes, as this phase began to form at 400 °C, 50 °C lower than the sample ground for 1 h. By 450 °C this broad reflection was well defined. However, the presence of the CuO phase in the 1 h sample could mask the development of the $CuMn_2O_4$ phase, as the broad $(\bar{1}\,1\,1)$ reflection of the CuO could be obscuring the $(3\,1\,1)$ reflection of the $CuMn_2O_4$. At 500 °C peaks corresponding to Mn_2O_3 are observed again in the 72 h ground sample. This is despite there being no corresponding CuO peak. Within the $CuMn_2O_4$ lattice there are vacant tetrahedral sites, as the ratio of Cu:Mn has been determined by EDX to be 1:2, the missing Cu could be located within these sites, or it remains as a dispersed amorphous phase.

The elemental analysis by MP-AES shows that the Cu:Mn ratio is remaining constant for the duration of the grinding process. The ratio of about 1:1.84 is slightly lower than the 1:2 that was expected, this could be due to the hygroscopic nature of the precursor materials. This also explains the slight deviations in the Cu:Mn ratio between the samples.

Temperature programmed reduction profiles of the calcined catalysts are shown in Fig. 6. The catalyst ground for 0.5 h exhibits one broad reduction peak at 297 °C with a prominent shoulder at 255 °C, this peak and is attributed to the reduction of CuO (as seen in the XRD) followed by the more complex reduction of residual $MnCO_3$ in combination with the partial formation and subsequent reduction of $Mn_2O_3 \rightarrow MnO$. CuO often exhibits a shoulder of this kind and this has been attributed to multiple CuO species existing in conjunction with other metal oxide species [36] and to amorphous CuO species [37]. After 1 h grinding the CuO reduction is still observed with the previous shoulder becoming a prominent peak at 254 °C. There is also a peak observed at 404 °C this can be attributed to the second step of the reduction of $Mn_2O_3 \rightarrow Mn_3O_4 \rightarrow MnO$. After 6 h of grinding the CuO peaks have shifted to lower temperatures with the presence of manganese phases observed. This is consistent with previous studies which show that the presence of Mn_2O_3 lowers the CuO reduction temperature from the pure

Table 2
Summary of data obtained from temperature programmed reduction studies calcined copper manganese oxide catalysts produced by mechanochemical grinding.

Time (h)	Hydrogen consumption (mol g^{-1})
0.5	0.018
1	0.016
12	0.018
24	0.016
72	0.024
Theoretical yield for $CuMn_2O_4$	0.021

$CuO \rightarrow Cu$ reduction [38]. As grinding time increased there was a gradual increase in the ease of reducibility of the manganese phases, indicated by the observation of the $Mn_2O_3 \rightarrow Mn_3O_4$ reduction at 292 °C and $Mn_3O_4 \rightarrow MnO$ at 390 °C. After 24 h grinding the reduction temperatures for all peaks continued to decrease. After 72 h grinding the reduction profile was typical of that of a spinel-type copper manganese mixed metal oxide, with a two stage reduction at 252 °C and 308 °C [38]. An observation is that there is a low temperature TPR shoulder observed that constantly shifts to lower reduction temperatures with increasing grinding time. If catalytic activity were associated with a redox mechanism [39,40] the prevalence of lower temperature reduction could be an indicator for superior catalytic activity, as the lability of lattice oxygen increases with greater grinding time.

TPR hydrogen consumption data are detailed in Table 2. The catalysts ground for 24 h, or less, all showed similar H_2 consumption. After 72 h the H_2 consumption increased by 50%. This increased extent of reduction is explained by the presence of the mixed $CuMn_2O_4$ phase without any residual carbonate or individual oxide phases.

SEM-EDX mapping was conducted to assess the homogeneity of the catalysts post calcination, and results support analysis from TPR and XRD. The catalyst ground for 0.5 h (Fig. 7a) showed large micron sized areas of phase separated copper and manganese material. The same type of phase segregated material was also observed after grinding for 1 h, but the copper rich regions were smaller in dimension (Fig. 7b). It can clearly be seen that efficient mixing on the micron scale is only achieved after grinding for 24 h (Fig. 7c), with the 72 h sample showing the most homogeneous dispersion of copper and manganese on the micron scale (Fig. 7d).

The catalysts were investigated using transmission electron microscopy in an attempt to determine mixing on the nanoscale (Fig. 8). Analysis of the calcined 72 h ground material can provide greater detail on the interaction of Cu and Mn phases after 415 °C calcination. Fig. 8a shows well defined crystalline lattice fringes. The spacing of these fringes (0.476 nm) closely corresponds to the (1 1 1) plane of $CuMn_2O_4$. Care should be taken as the (1 0 1) plane of Mn_3O_4 has a similar d-spacing (0.492 nm), however, no evidence of this phase is observed by any of the other characterization techniques. Additionally lattice spacings of 0.243 and 0.257 nm were also determined and closely correspond to the (1 1 1) and (3 1 1) planes of $CuMn_2O_4$. The EDX analysis (Fig. 8b) clearly shows that despite the prolonged grinding there are still distinct grains of copper rich material and grains of manganese rich material with the mixed phase which predominantly exists between the grains. This reinforces our suggestion that the formation of the mixed phase requires close association of the manganese and copper species. The friction between the grains during the milling process could be important to provide the energy to start the copper species migrating into the manganese lattice.

All materials calcined at 415 °C were used as catalysts for CO oxidation at ambient temperature (25 °C). The results are presented in Fig. 9 and summarized in Table 3. What is immediately apparent is that even after 0.5 h grinding the catalyst was able to oxidize CO with 10% conversion to CO_2. The individual copper and

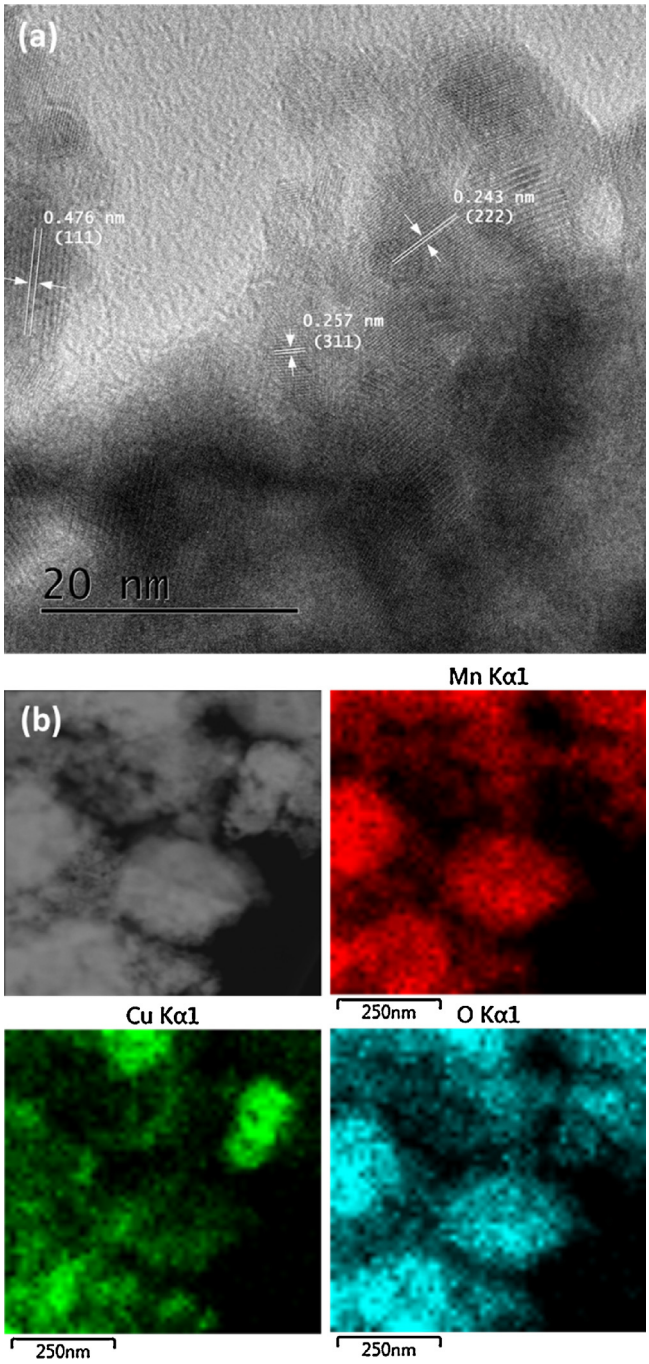

Fig. 8. Transmission Electron Microscopy analysis: (a) Representative TEM image showing crystalline lattice fringes and amorphous material. (b) STEM and representative EDX mapping of sample ground for 72 h showing manganese (red) and copper (green) and oxygen blue.

manganese oxides are known to be active for CO conversion [41], as are mixtures of these phases, and it has been previously argued that a mixture of CuO, MnO_2 and $CuMn_2O_4$ are necessary for optimum activity [25,26]. Some have suggested that at elevated temperature the combination of phases are important as the catalyst operates by a spillover will influence the mechanism of CO oxidation.

The catalysts ground up to 24 h showed relatively low levels of activity (*ca.* 10%). The EDX and XRD data indicate that catalysts ground for up to 24 h are still largely phase separated CuO and $MnCO_3$, probably containing partially formed isolated $CuMnO_x$ domains, resulting in moderate but stable activity. The individual copper and manganese oxides (Table 2) showed no activity for

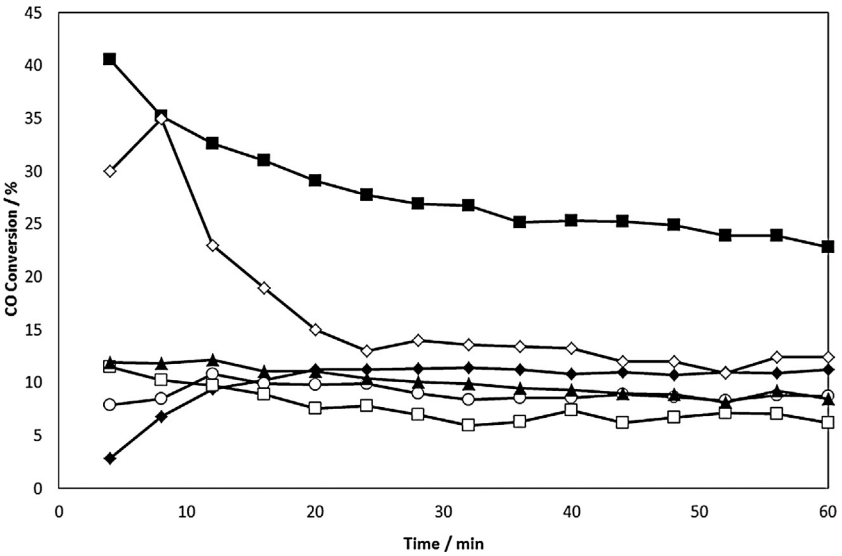

Fig. 9. Time-on-line data for the conversion of CO to CO_2: ♦ 0.5 h, ○ 1 h, □ 12 h, ▲ 24 h, ■ 72 h, ◊ Commercial catalyst. (25 °C, 12000 h^{-1}, 5000 ppm CO in synthetic air).

Table 3
Catalytic activity of calcined copper manganese oxide catalysts produced by mechanochemical grinding.

Catalyst	Steady state activity[a] (%)	Calcined surface area ($m^2\ g^{-1}$)	Surface area normalised rates at steady state ($mol\ s^{-1}\ m^{-2}$)[a]
0.5 h	11	65	1.76×10^{-7}
1 h	6	45	2.52×10^{-7}
12 h	12	50	1.26×10^{-7}
24 h	8	21	4.09×10^{-7}
72 h	23	78	2.97×10^{-7}
Commercial catalyst	12	140	0.90×10^{-7}
CuO	0	–	–
Mn_2O_3	0	–	–

[a]Data taken from activity of materials after on one hour of testing.

the oxidation of CO suggesting that some of the $CuMn_2O_4$ species has been formed in even the catalysts ground for relatively short periods of time and it is responsible for the observed activity. After grinding for 72 h the CO conversion increased significantly, becoming stable at approximately 23% conversion after 60 min on-line. Taken in conjunction with the characterization data, it suggests that $CuMn_2O_4$ is the active phase. This activity is roughly double the steady state activity of a commercial copper manganese oxide catalyst used for CO oxidation Fig. 9 and Table 3.

The initial activity of the commercial catalyst is similar to the catalyst ground for 72 h. However the activity drops rapidly due to deactivation by water adsorption [42]. The temperature of the catalyst bed was maintained at 25 °C so the deactivation could not have been obscured by a rise in the temperature of the catalyst bed. The deactivation of copper manganese oxide catalysts by water at low temperatures is not a subject that is well understood however it is of note that the mechanochemically prepared samples appear to have some resistance to it.

Catalysts ground for less than 24 h all have relatively similar surface area normalized rates with activity mainly attributed to isolated CuMnOx domains. The decrease in surface area after 24 h grinding contributes to this catalyst having the highest CO oxidation activity per unit surface area (Fig. 10). It is difficult to draw any definitive conclusions from the surface area normalized rates, as characterization showed that the catalysts contained varying amounts of inactive CuO and $MnCO_3$, effectively acting as catalyst diluent.

The results presented all support the hypothesis that the mixed $CuMn_2O_4$ phase is required for appreciable levels of CO oxidation at ambient temperature. No evidence of the individual component

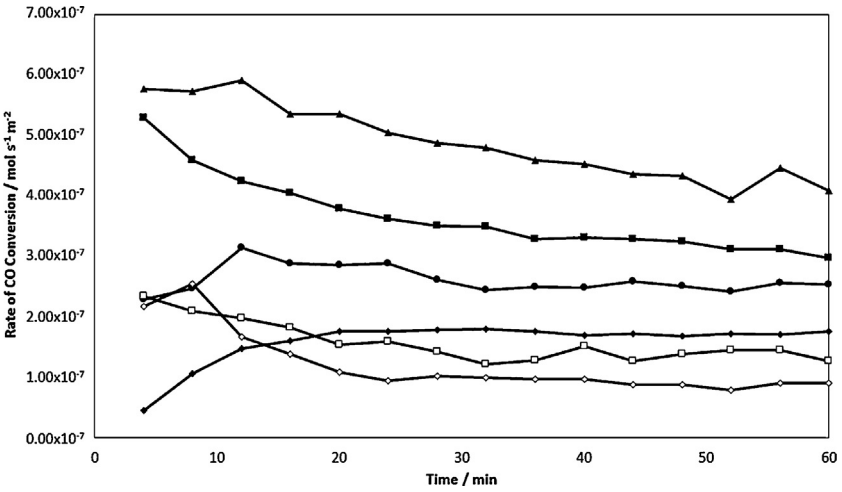

Fig. 10. Surface area normalized time-on-line data for the conversion of CO to CO_2: ♦ 0.5 h, ○ 1 h, □ 12 h, ▲ 24 h, ■ 72 h. (25 °C, 12000 h^{-1} 5000 ppm CO in synthetic air).

metal oxides was seen in the material ground for 72 h. This fact, coupled with the very low activity of the catalysts ground for shorter periods and inactivity of the individual oxide materials leads to the conclusion that it is the $CuMn_2O_4$ species that is the active species in this case and that a proposed spillover mechanism is not responsible for the CO activity of the catalyst [38].

4. Conclusion

It has been shown that an active low temperature CO oxidation catalyst can be prepared by a one-step mechanical grinding of copper and manganese carbonate precursors, with the advantage that no aqueous waste is generated. Under our test conditions this catalyst out performs the commercial catalyst. We demonstrate that incorporation of Cu^{2+} into the $MnCO_3$ lattice to form $Cu_xMn_{1-x}CO_3$ is an important factor in the formation of the active $CuMn_2O_4$ phase upon calcination and the possibility of its formation should be considered when discussing the nature of the Hopcalite precursor. It is possible that an undetected stabilized amorphous copper species exists alongside this mixed carbonate phase. We show that the incorporation of Cu^{2+} ions into the $MnCO_3$ framework is dependent upon grinding time, and the presence of Cu^{2+} within the $MnCO_3$ lattice consequently facilitates the formation of the active $CuMn_2O_4$ phase upon calcination. *In situ* XRD suggests the active $CuMn_2O_4$ phase is formed from this mixed carbonate species rather than from a reaction of the individual oxides. The extent of Cu^{2+} incorporation into the $MnCO_3$ lattice can be followed by XRD by monitoring the shift in the position of the $MnCO_3$ (1 0 4) reflection. Results suggest that the migration of Cu^{2+} ions into the $MnCO_3$ lattice during the mechanochemical reaction appears to be a thermodynamically favoured, but kinetically limited process. Forming an active $CuMn_2O_4$ catalyst by the mechanochemical method, we have demonstrated, removes many of the poorly understood variables associated with a process like co-precipitation. Mechanochemical preparation also has no need for an alkali metal carbonate precipitating agent, eliminating a major source of catalyst poison, and a stream of aqueous waste.

Acknowledgements

The authors would like to acknowledge the help of Jenny Holter and the Science and Technology Facilities Council for the microscopy facilities at Harwell research campus.

Appendix A. Supplementary data

Supplementary data associated with this article can be found, in the online version, at http://dx.doi.org/10.1016/j.apcatb.2014.09.070.

References

[1] K. Ralphs, C. Hardacre, S.L. James, Chem. Soc. Rev. (2013).
[2] P. Baláž, A. Aláčová, M. Achimovičová, J. Ficeriová, E. Godočíková, Hydrometallurgy 77 (2005) 9–17.
[3] A. Rougier, S. Soiron, I. Haihal, L. Aymard, B. Taouk, J.M. Tarascon, Powder Technol. 128 (2002) 139–147.
[4] V.V. Molchanov, R.A. Buyanov, Y.T. Pavlyukhin, Kinet. Catal. 44 (2003) 788–792.
[5] P.J. Sanchez-Soto, A. Wiewióra, M.A. Avilés, A. Justo, L.A. Pérez-Maqueda, J.L. Pérez-Rodríguez, P. Bylina, Appl. Clay Sci. 12 (1997) 297–312.
[6] T.E. Davies, T. Garcia, B. Solsona, S.H. Taylor, Chem. Commun. (2006) 3417–3419.
[7] H. Yang, Y. Hu, X. Zhang, G. Qiu, Mater. Lett. 58 (2004) 387–389.
[8] S.K. Pardeshi, A.B. Patil, J. Mol. Catal. A: Chem. 308 (2009) 32–40.
[9] I.-C. Kang, Q. Zhang, S. Yin, T. Sato, F. Saito, Appl. Catal. B: Environ. 80 (2008) 81–87.
[10] P. Billik, G. Plesch, V. Brezová, L. Kuchta, M. Valko, M. Mazúr, J. Phys. Chem. Solids 68 (2007) 1112–1116.
[11] K. Wieczorek-Ciurowa, J. Rakoczy, A. Błońska-Tabero, E. Filipek, J. Nizioł, P. Dulian, Catal. Today 176 (2011) 314–317.
[12] J. Rakoczy, J. Nizioł, K. Wieczorek-Ciurowa, P. Dulian, Mech. Catal. 108 (2013) 81–89.
[13] H.L. Castricum, H. Bakker, B. van der Linden, E.K. Poels, J. Phys. Chem. B 105 (2001) 7928–7937.
[14] L.C. Wang, Y.M. Liu, Y. Cao, G.S. Wu, C.Z. Yao, W.L. Dai, H.Y. He, K.N. Fan, Acta Chim. Sin. 65 (2007) 173–176.
[15] L.C. Wang, Y.M. Liu, M. Chen, Y. Cao, H.Y. He, G.S. Wu, W.L. Dai, K.N. Fan, J. Catal. 246 (2007) 193–204.
[16] N.G. Kostova, A.A. Spojakina, E. Dutková, P. Baláž, J. Phys. Chem. Solids 68 (2007) 1169–1172.
[17] L. Ilieva, G. Pantaleo, I. Ivanov, R. Zanella, A.M. Venezia, D. Andreeva, Int. J. Hydrogen Energy 34 (2009) 6505–6515.
[18] S.A. Kondrat, G. Shaw, S.J. Freakley, Q. He, J. Hampton, J.K. Edwards, P.J. Miedziak, T.E. Davies, A.F. Carley, S.H. Taylor, C.J. Kiely, G.J. Hutchings, Chem. Sci. 3 (2012) 2965–2971.
[19] S. Kaliaguine, A. Van Neste, V. Szabo, J.E. Gallot, M. Bassir, R. Muzychuk, Appl. Catal. A: Gen. 209 (2001) 345–358.
[20] V. Szabo, M. Bassir, A. Van Neste, S. Kaliaguine, Appl. Catal. B: Environ. 37 (2002) 175–180.
[21] Y.-s. Lee, Y.-K. Sun, K.-S. Nahm, Solid State Ionics 109 (1998) 285–294.
[22] W. Kim, F. Saito, Powder Technol. 113 (2000) 109–113.
[23] J.K. Musick, F.W. Williams, Product R&D 14 (1975) 284–286.
[24] A.B. Lamb, W.C. Bray, J.C.W. Fraser, J. Ind. Eng. Chem. (Washington, D. C.) 13 (1920) 213–221.
[25] G.J. Hutchings, A.A. Mirzaei, R.W. Joyner, M.R.H. Siddiqui, S.H. Taylor, Appl. Catal. A: Gen. 166 (1998) 143–152.
[26] C. Jones, K.J. Cole, S.H. Taylor, M.J. Crudace, G.J. Hutchings, J. Mol. Catal. A: Chem. 305 (2009) 121–124.
[27] A.A. Mirzaei, H.R. Shaterian, M. Habibi, G.J. Hutchings, S.H. Taylor, Appl. Catal. A: Gen. 253 (2003) 499–508.
[28] M. Krämer, T. Schmidt, K. Stöwe, W.F. Maier, Appl. Catal. A: Gen. 302 (2006) 257–263.
[29] Z.-R. Tang, C.D. Jones, J.K.W. Aldridge, T.E. Davies, J.K. Bartley, A.F. Carley, S.H. Taylor, M. Allix, C. Dickinson, M.J. Rosseinsky, J.B. Claridge, Z. Xu, M.J. Crudace, G.J. Hutchings, ChemCatChem 1 (2009) 247–251.
[30] R.P. Marin, S.A. Kondrat, R.K. Pinnell, T.E. Davies, S. Golunski, J.K. Bartley, G.J. Hutchings, S.H. Taylor, Appl. Catal. B: Environ. 140–141 (2013) 671–679.
[31] Z.R. Tang, S.A. Kondrat, C. Dickinson, J.K. Bartley, A.F. Carley, S.H. Taylor, T.E. Davies, M. Allix, M.J. Rosseinsky, J.B. Claridge, Z. Xu, S. Romani, M.J. Crudace, G.J. Hutchings, Catal. Sci. Technol. 1 (2011) 740–746.
[32] S.A. Kondrat, T.E. Davies, Z. Zu, P. Boldrin, J.K. Bartley, A.F. Carley, S.H. Taylor, M.J. Rosseinsky, G.J. Hutchings, J. Catal. 281 (2011) 279–289.
[33] P. Porta, G. Moretti, M.L. Jacono, M. Musicanti, A. Nardella, J. Mater. Chem. 1 (1991) 129–135.
[34] Q. Zhang, F. Saito, J. Mater. Sci. 36 (2001) 2287–2290.
[35] A.F. Rogers, J. Geol. 25 (1917) 515–541.
[36] G. Fierro, M. Lojacono, M. Inversi, P. Porta, R. Lavecchia, F. Cioci, J. Catal. 148 (1994) 709–721.
[37] KALCHEV, M. G., ANDREEV, A. A., ZOTOV, N. S., Water-gas shift reaction on CuO;ZnO catalysts. I: Structure and catalytic activity, Maik Nauka/Interperiodica, Moscow, RUSSIE, FEDERATION DE, 1995.
[38] F.C. Buciuman, F. Patcas, T. Hahn, Chem. Eng. Process. Proc. Intens. 38 (1999) 563–569.
[39] G.M. Schwab, S.B., Kanugo, Z., Phys, Chem, 107 (1977) 109.
[40] S.B. Kanungo, J. Catal. 58 (1979) 419–435.
[41] U.R. Pillai, S. Deevi, Appl. Catal. B: Environ. 64 (2006) 146–151.
[42] E.C. Njagi, C.-H. Chen, H. Genuino, H. Galindo, H. Huang, S.L. Suib, Appl. Catal. B: Environ. 99 (2010) 103–110.